Electronic Supplementary Material (ESI) for Journal of Materials Chemistry C.

Supporting Material

XRD

As shown in Figure 1 all samples contain MgO as impurity. Due to the high reactivity of Mg with oxygen this is usually observed in Mg2Si based materials. A zoom in of the XRD data around the MgO main peak is shown in Figure S1.

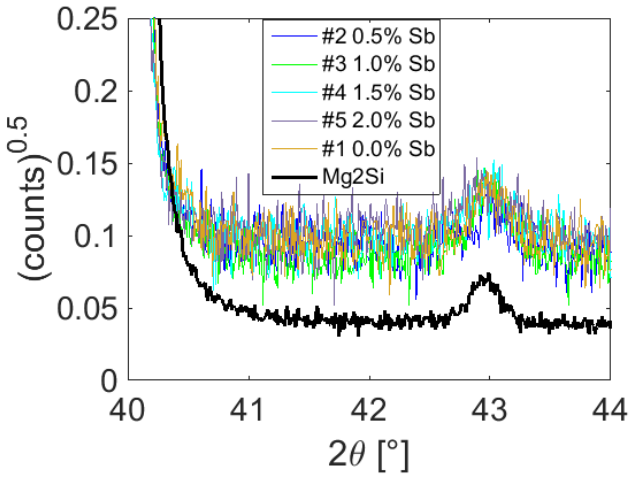

Figure S1: X-ray diffraction data around the MgO main peak.

The peak height and area of the MgO main peak is comparable for all Mg2Si0.8sn0.2 samples, indicating similar MgO amounts. Comparison with the Mg2Si sample shows a small increase for the Sn containing samples. Indeed a Rietveld refinement using the same parameters for MgO in all samples yields comparable numbers for the Mg2Si0.8Sn0.2 samples and a slightly lower MgO content for the Mg2Si sample that is shown as reference.
The observed MgO is one likely cause for the reduced electrical conductivity and mobility observed at 300- 450 K.

Micrographs

Depicted below are several electron microscope images. The compositional results from EDX analysis are given as well. Note that the Sb-content is highly inaccurate due to the similarity of the spectra for Sn and Sb. The Sn content x is estimated using $x = \frac{\%Sn}{\%Si + \%Sn}$, i.e. ignoring the dopant.

Mg2Si0.8Sn0.2

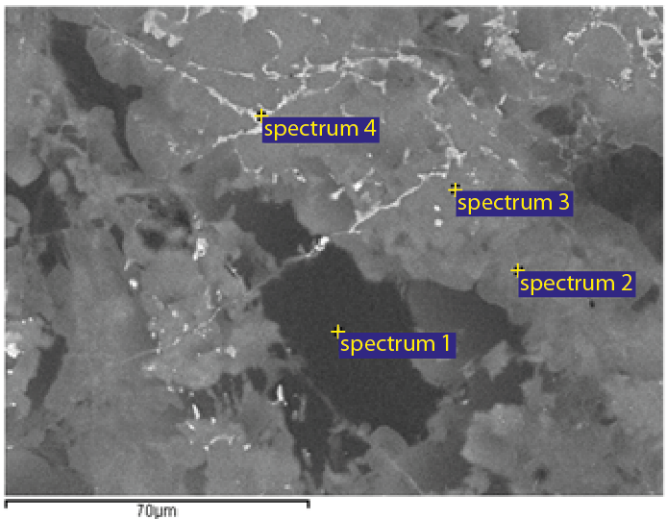

Figure S2

Point	Phase	Mg	Si	Sn	Sn content x
spectrum 1	β	65.9	33.4	0.68	0.02
spectrum 2	α	65.9	27.3	6.7	0.20
spectrum 3	α	65.5	27.1	7.4	0.21
spectrum 4	γ	65.4	14.7	19.9	0.58

$Mg_2Si_{0.79}Sn_{0.2}Sb_{0.01}$

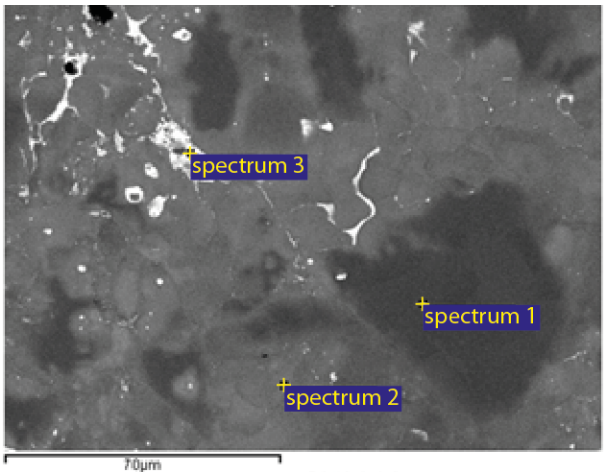

Figure S3

Point	Phase	Mg	Si	Sn	Sb	Sn content x
spectrum 1	β	66.16	32.63	0.81	0.39	0.02
spectrum 2	α	66.14	29.26	4.33	0.27	0.13
spectrum 3	γ+MgO					

Mg2Si0.78Sn0.2Sb0.02 (sample #5)

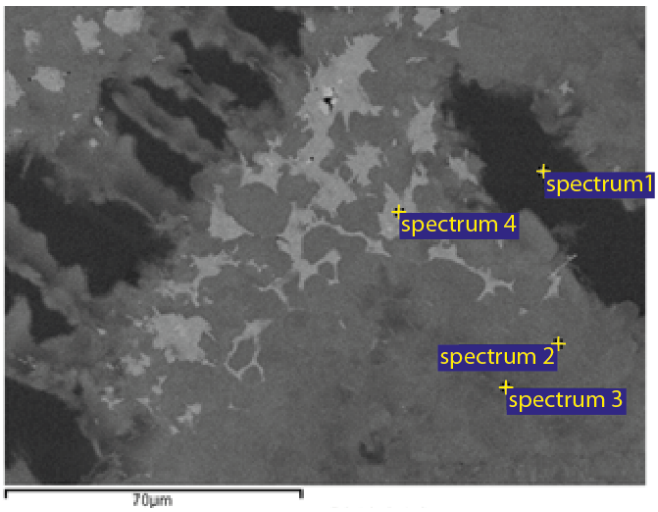

Figure S4

Point	Phase	Mg	Si	Sn	Sb	Sn content x
spectrum 1	β	65.9	32.4	0.9	0.7	0.03
spectrum 2	α	65.7	27.2	6.4	0.7	0.19
spectrum 3	α	65.7	29.3	4.5	0.6	0.13

spectrum 4	γ	65.6	18.9	15.6	0.45

Transport data for the undoped sample (#1)

The transport data of the (nominally) undoped sample (#1) is shown in Figure S5. The electrical conductivity first decreases and then decreases rapidly above 550 K, while the opposite is true for the Seebeck effect. This are the expected trends for a sample going from extrinsic conduction (caused by inevitable unintentional doping during the synthesis) to intrinsic conduction, where carriers are thermally excited above the band edge. In the thermal conductivity the onset of bipolar thermal transport is clearly visible. The resulting ZT is roughly one order of magnitude less than for the doped samples.

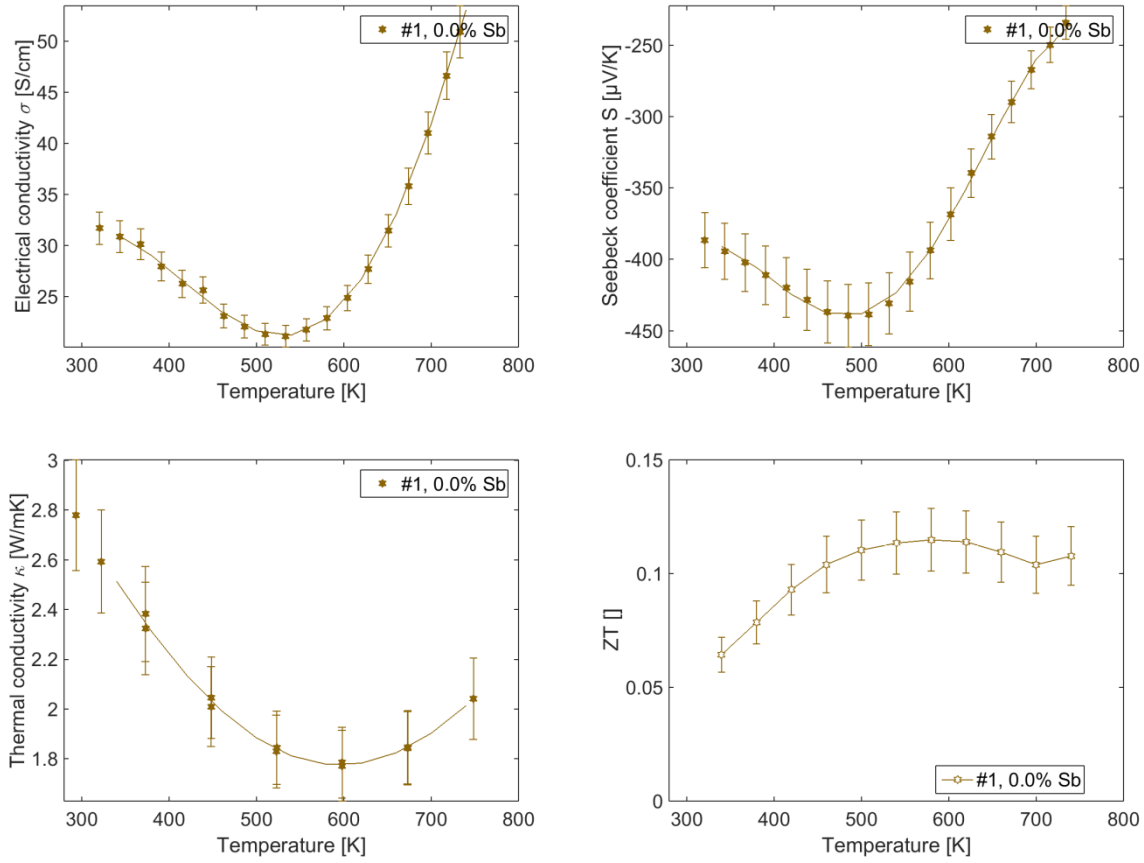

Figure S5: Thermoelectric transport properties for sample #1 with nominal stoichiometry $Mg_2Si_{0.8}Sn_{0.2}$ and no Sb doping.

Sample homogeneity

We have also checked sample homogeneity by a local mapping of the Seebeck coefficient (for details on the technique see e.g. [1]). The result for #4 is shown below.

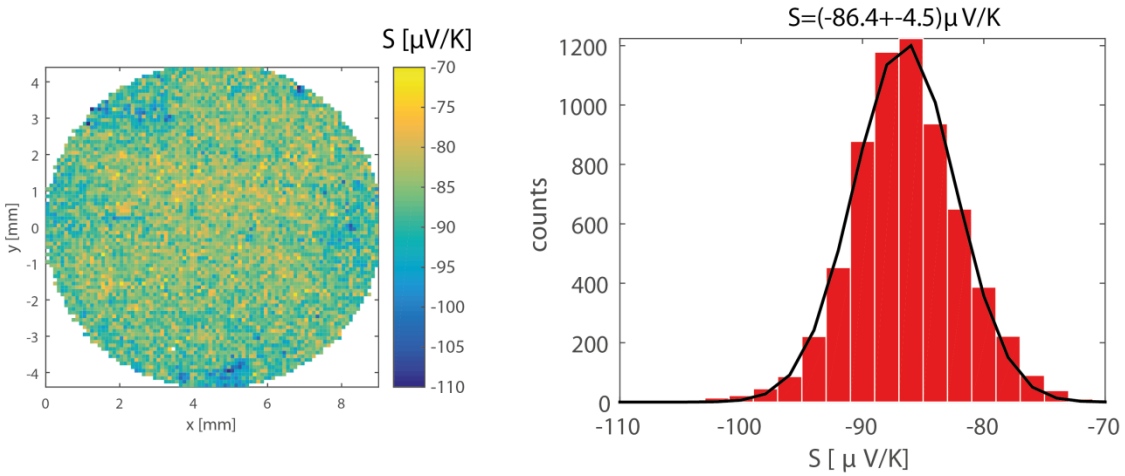

Figure S6: local Mapping of the Seebeck coefficient of sample #4.

It can be seen that the sample shows some fluctuations on the 100µm scale as well as some small regions with higher Seebeck coefficient at the outer part. Nevertheless the homogeneity displayed here as well as the peak half width with $\approx 5\%$ is typical for sintered thermoelectric materials. The average value of $-86\ \mu V/K$ at room temperature agrees well with the result from the temperature dependent, integral measurement as displayed in Figure 4.

Single parabolic band model

The measured Hall carrier density n_H is linked to the true carrier density by $n_H = n/r_H$ with the Hall scattering factor given by $r_H = \frac{1.5F_{0.5}F_{-0.5}}{2F_0^2}$. The true carrier density shows a stronger apparent increase with temperature than the Hall carrier density. The increase is not due to intrinsic charge carriers and probably unphysical. We believe that it is due to the non-parabolicity of the lower conduction band that is not taken into account in the SPB model.

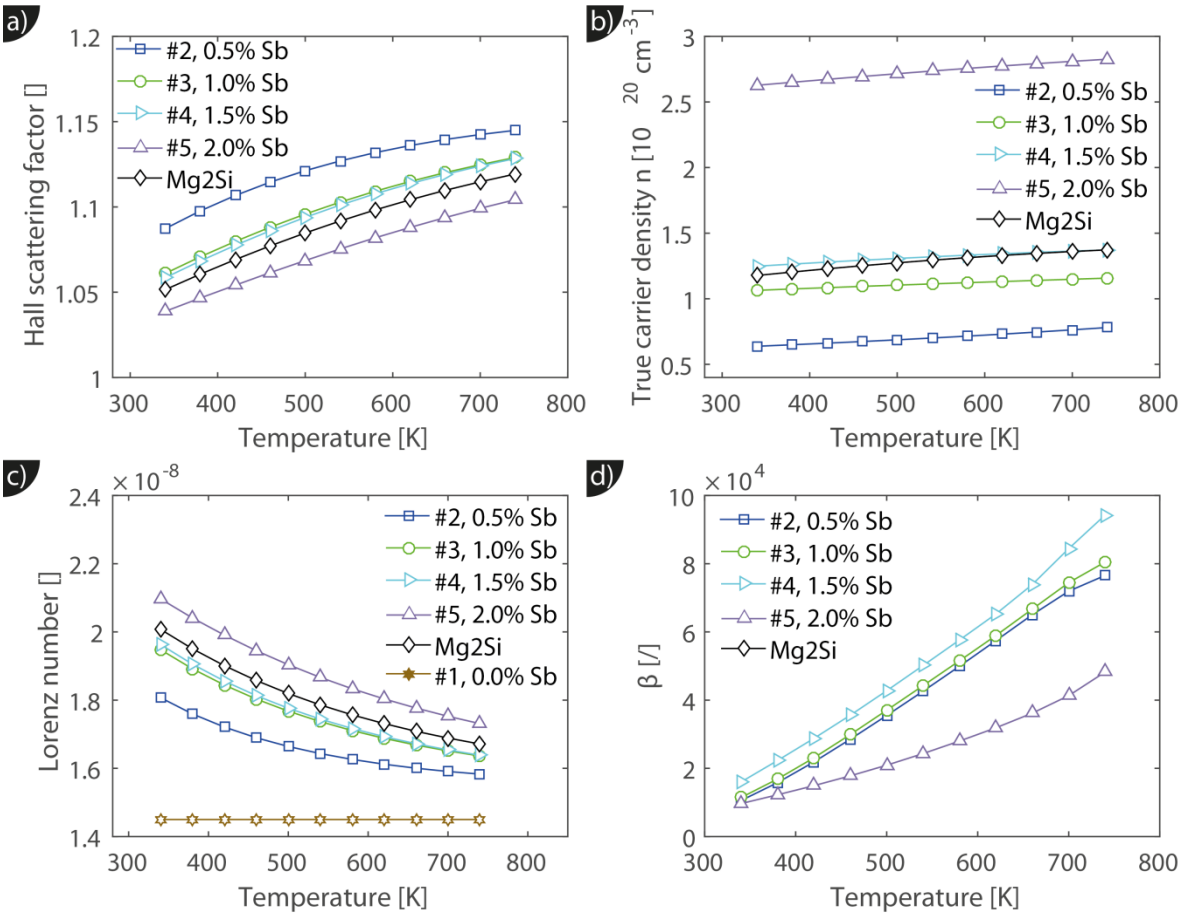

Figure S7: Further parameters from the SPB model

$$L = \frac{k^2 3F_0F_2 - 4F_1^2}{e^2 \quad F_0^2}$$

The Lorenz number is calculated using for the doped samples. For the undoped sample the non-degenerate limit $L = 1.45 * 10^{-8} W\Omega K^{-2}$ was employed.

References

1. P. Ziolkowski, G. Karpinski, T. Dasgupta and E. Muller, *Phys. Status Solidi A-Appl. Mat.*, 2013, **210**, 89-105.